Microfluid Nanofluid (2009) 6:637–646
DOI 10.1007/s10404-008-0339-8

RESEARCH PAPER

Experiments on opto-electrically generated microfluidic vortices

Aloke Kumar · Stuart J. Williams · Steven T. Wereley

Received: 2 June 2008 / Accepted: 23 July 2008 / Published online: 23 August 2008

Abstract Strong microfluidic vortices are generated when a near-infrared (1,064 nm) laser beam is focused within a microchannel and an alternating current (AC) electric field is simultaneously applied. The electric field is generated from a parallel-plate, indium tin oxide (ITO) electrodes separated by 50 μm. We present the first μ-PIV analysis of the flow structure of such vortices. The vortices exhibit a sink-type behavior in the plane normal to the electric field and the flow speeds are characterized as a function of the electric field strength and biasing AC signal frequency. At a constant AC frequency of 100 kHz, the fluid velocity increases as the square of the electric field strength. At constant electric field strength fluid velocity does not change appreciably in the 30–50 kHz range and it decreases at larger frequencies (>1 MHz) until at approximately 5 MHz when Brownian motion dominates the movement of the 300 nm μ-PIV tracer particles. Presence of strongly focused laser beams in an interdigitated-electrode configuration can also lead to strong microfluidic vortices. When the center of the illumination is focused in the middle of an electrode strip, particles experiencing negative dielectrophoresis are carried towards the illumination and aggregate in this area.

Keywords MicroTAS · Opto-electrostatic micro vortex · Micropump · Electrohydrodynamics · Dielectrophoresis

A. Kumar · S. J. Williams · S. T. Wereley (✉)
Birck Nanotechnology Center and School of Mechanical Engineering, Purdue University,
West Lafayette, IN 47907, USA
e-mail: wereley@purdue.edu

A. Kumar
e-mail: kumar31@purdue.edu

1 Introduction

Precisely controlling fluids and particles at the micro- and nano-scales are important for the development of microfluidic total analysis systems (μ-TAS) (Koch et al. 2000) and Lab-on-a-chip type systems (Figeys and Pinto 2000). Of the various methods that have been developed, AC electrokinetic techniques can be integrated into microsystems with basic fabricated microelectrode structures and can be controlled by changing the applied signal potential and frequency. Electrohydrodynamic techniques include AC electro-osmotic pumping, in which the electric field acts upon the ionic double layer of the fluid inducing motion on the electrode surface (Müller et al. 1996; Trau et al. 1997; Ramos et al. 1998), and eletrothermal pumping, where the field acts upon temperature-induced gradients in electrical permittivity and conductivity resulting in bulk fluid motion (Green et al. 2000, 2001). Dielectrophoresis (DEP) is a popular electrokinetic microparticle manipulation technique that refers to the induced force exerted on a dielectric particle due to their interaction with a non-uniform electric field (Pohl 1978; Jones 1995). These electrokinetic techniques are driven with potentials typically under 20 V peak-to-peak (V_{pp}) and frequencies under 10 MHz (Morgan and Green 2003).

The need for multiplexing in order to simultaneously analyze multiple samples (Figeys and Pinto 2000) is leading to the development of novel bulk fluid and particle manipulation techniques and their incorporation onto Lab-on-a-chip devices. Optically-induced electrokinetic methods offer one potential technique. Recent strides in the area of dynamic electrode generation (Chiou et al. 2005; Hwang et al. 2008) have demonstrated that light can be used to define 'virtual' electrode structures which dielectrophoretically manipulate particles on a massive scale.

Optical tweezers (OT) employ highly focused laser beams for trapping particles, typically only one particle at a time (Ashkin et al. 1987). In order to couple OT with DEP, it is important to understand the effect of illumination in the presence of electric fields. The illumination itself will heat the fluid sample resulting in electrothermally-induced fluid motion. OTs have been used simultaneously with DEP previously (Fuhr et al. 1998; Reichle et al. 2000; Schnelle et al. 2000; Reichle et al. 2001; Simpson et al. 2002; Rowe et al. 2003; Papagiakoumou et al. 2006), typically one technique was used to quantify the strength or efficiency of the other. However, electrothermal effects from the OT illumination were not discussed.

1.1 Current studies in optically induced electrothermal flows

Mizuno et al. (1995) first observed strong vortices driven by an electric field interacting with local fluid temperature gradients generated from laser-induced heating. The researchers used a focused YAG laser operating at 1,064 nm and presented flow visualization results of a microvortex they termed an opto-electrostatic microvortex (OEMV). They illustrated the microvortex as predominantly two-dimensional in structure. Green et al. (2000) produced electrohydrodynamic effects with a broad illumination source and, in a later work (Green et al. 2001), the researchers presented an electro-hydrodynamic analysis of such temperature-induced electrohydrodynamic flows. In a recent work, OEMV was used as a microfluidic pump (Nakano et al. 2007). The relatively high induced fluid velocities ($\sim$100 μm/s) and low cost of manufacture make these OEMV pumps favorable (Nakano et al. 2007). It is important to note that while these previous investigations employed different types of illumination, the electrode structures were coplanar in both cases. The electric field for this arrangement is not completely uniform, especially near the electrode edges, complicating experimental analyses.

1.2 Aims and scope of present work

We explore fluid flows in a simple parallel-plate electrode geometry, with the intention of increasing the experimental analysis of OEMV and similar flows. We present evidence of the three-dimensional nature of the microvortex and a detailed two-dimensional micron resolution particle image velocimetry (μ-PIV) analysis of the same is carried out in a plane parallel to the electrodes. The electrode setup was motivated by the intention to create uniform electric fields that do not inherently possess non-uniform field gradients that would induce dielectrophoretic forces on tracer particles.

We also investigate the behavior of these microfluidic vortices with an interdigitated electrode setup. Velocimetry studies were not performed as this electrode geometry exerts considerable dielectrophoretic forces on tracer particles. However, effects of opto-electrokinetically generated vortices are studied in order to assess their impact on dielectrophoretic particle capture. Our investigation of illumination-induced electrothermal fluid flow with interdigitated electrodes differs from previous experiments using a coplanar electrode pair (Green et al. 2000). First, our illumination source is a highly focused laser beam typically associated with optical tweezers while their investigation used uniform illumination. Second, interdigitated electrodes are a popular electrokinetic geometry in Lab-on-a-chip systems compared to a single coplanar electrodes arrangement. Most important, this work provides experimental measurements to compare with expected behavior from theory (Ramos et al. 1998; Green et al. 2001; Chakraborty 2008).

2 Electrothermal flows

Localized fluid heating generates gradients in electrical permittivity and conductivity. An applied electric field acts on these gradients, inducing a body force acting on the fluid. The time-averaged expression for this body force (f_e) is (Green et al. 2001):

$$\langle f_e \rangle = 1/2\,\mathrm{Re}\left[\frac{\sigma\varepsilon(\alpha-\beta)}{\sigma+i\omega\varepsilon}(\nabla T\cdot \boldsymbol{E_o})\boldsymbol{E_o^*} - 1/2\varepsilon\alpha|\boldsymbol{E_o}|^2\nabla T\right] \quad (1)$$

where Re refers the real part of the expression, $\boldsymbol{E_o}$ is the electric field, $\boldsymbol{E_o^*}$ is its complex conjugate, T is the temperature, ω is the applied frequency, σ and ε are the conductivity and permittivity of the fluid, respectively, β is $\left(1/\sigma \mathrm{d}\sigma/\mathrm{d}T\right)$, and α is $\left(1/\varepsilon \mathrm{d}\varepsilon/\mathrm{d}T\right)$. The first term in Eq. (1) is the Coulomb force and the second term is the dielectric force and the latter term will dominate as the applied AC frequency increases. Note that each term is dependent on local temperature gradients (∇T). The electric field itself generates heat that can contribute to this fluid body force. However, due to the uniform electric field intensity within a parallel-plate electrode configuration, the dominant source of non-uniform heat from our experiments comes from the highly focused optical illumination. This heating is non-uniform due to the highly-focused light patterns that vary radically in intensity over a few micrometers. The velocity of the OEMV depends on the illumination intensity, the dielectric properties of the fluid, and the applied AC signal.

Here we characterize the behavior of the OEMV by varying the applied AC voltage and frequency.

3 DEP with interdigitated electrodes

DEP refers to the translational motion of electrically neutral, dielectric particles due to their interaction with a non-uniform electric field (Pohl 1978). In the presence of an electric field the particle will polarize; if the electric field is non-uniform these induced forces are unbalanced resulting in particle translation. The magnitude and direction of the dielectric force is dependent on the dielectric properties of the fluid and particle. In an AC electric field, the particles can move towards the location of the greatest non-uniform field strength (positive DEP) or can be repelled from these non-uniform regions (negative DEP). Interdigitated electrodes are a novel configuration that can be used to determine whether a particle exhibits positive or negative DEP (Fig. 1). This geometry creates strong electric field gradients at the edges of the electrodes and particles experiencing positive DEP are attracted here. Particles experiencing negative DEP are repelled from these regions, away from the electrode substrate. If the height of the channel is relatively close to the electrode substrate the negative DEP particles will accumulate on the opposite wall, aligned with the middle of the electrode strips.

The interdigitated electrodes complicate the electrohydrodynamics of the OEMV. Unlike a parallel-plate electrode setup, the magnitude and direction of the electric field changes dramatically depending on the location. Similarly, the behavior of the OEMV within an interdigitated electrode setup will vary with the location of the illumination spot. In addition, the non-uniform electric field generates non-uniform heating and, with simultaneous illumination, this further complicates the thermal landscape. The final location of particles within an interdigitated electrode system with OEMV involves a balance of DEP, fluid drag, and buoyancy forces.

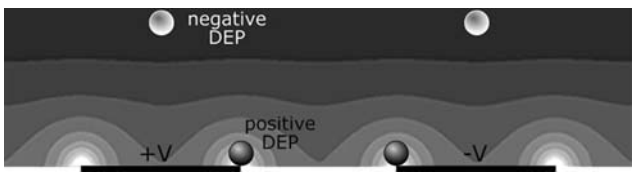

Fig. 1 Interdigitated electrodes for dielectrophoresis. The *grayscale* contour represents the electric field, with non-uniform regions at the electrode edges. Particles experiencing positive DEP are attracted to these non-uniform regions. Particles experiencing negative DEP are repelled from these regions and, if the height chamber is relatively low, they are located above the middle of the electrode digits

4 Visualizing three-dimensional transport with defocused particles

Induced microvortices in our parallel electrode setup exhibit a prominent three-dimensional flow structure. Imaging a point source in focus through a microscope results in an Airy disk pattern. For practical purposes, the Airy disk is well approximated by a Gaussian profile. As such fluorescent particles in focus appear as a spot (Fig. 2a) with the illumination intensity decreasing as radius increases. Particles that are out of focus display a ring pattern, which is caused both by diffraction and spherical lens aberration (Inouâe and Spring 1997) (Fig. 2b). The size of these rings gives insight into their distance from the focal plane. In case of video microscopy, three-

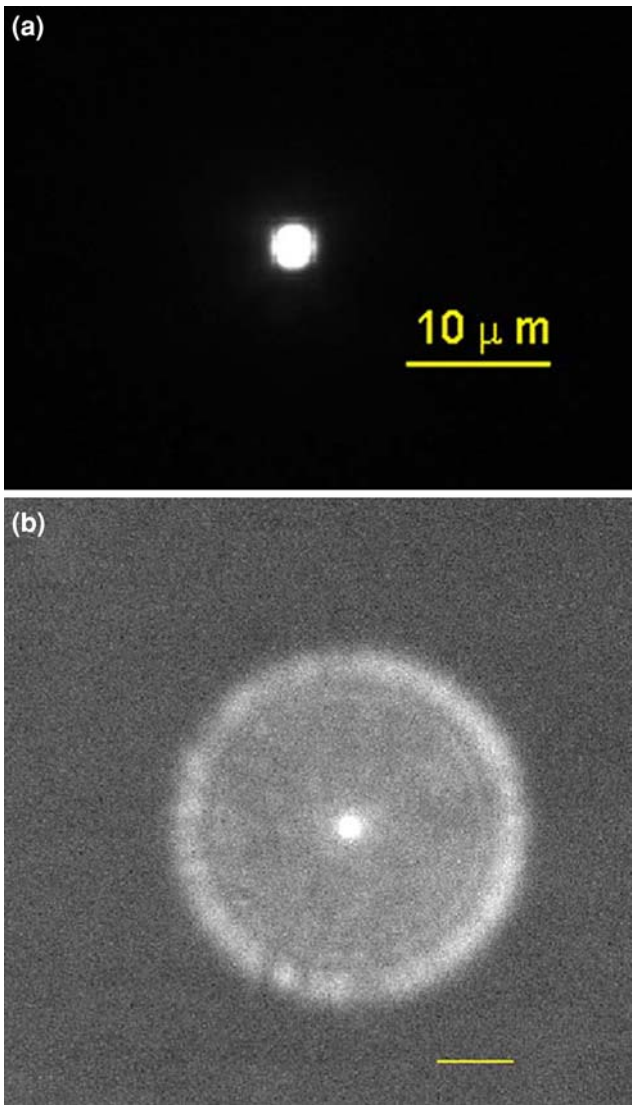

Fig. 2 Fluorescent imaging of focused and defocused particles with a 60× water immersion lens (numerical aperture-1.2). **a** A 2 μm bead which is in focus. **b** The same bead is placed 30 μm out of focus

dimensional transport often can be visualized by observing the changing ring pattern of the particle image. As a particle leaves the focal plane it becomes 'defocused' and the ring pattern becomes more prominent. It is possible to use this defocused particle image to track the out-of-plane position of the particle. Three-dimensional particle tracking techniques are being developed (Wu et al. 2005; Luo et al. 2006a, b). Particle tracking is a methodology of visualizing and quantifying fluid flow behavior by analyzing individual tracer particle images and determining their velocities. Compared to particle image velocimetry (PIV) it is a Lagrangian approach and algorithmically it is significantly different from the spatial cross-correlation approach of PIV.

5 Micron-resolution particle image velocimetry (μ-PIV)

For the parallel electrode configuration two-dimensional microscale velocimetry measurements are carried out using μ-PIV. μ-PIV today has become an extremely important and preferred tool to measure and diagnose microfluidic flows (Curtin et al. 2006; Pickard et al. 2006). μ-PIV is an adaptation of the macroscopic particle image velocimetry (PIV) technique, which has become almost ubiquitous today in experimental flow quantification. μ-PIV was first proposed in 1998 (Santiago et al. 1998). Like macroscopic PIV, μ-PIV acquires a series of images of seeded particles that follow fluid motion. Statistical tools are used to analyze the images and produce velocity vectors. Since the first experimental demonstrations of micron resolution PIV (Santiago et al. 1998), advanced algorithms were proposed to improve accuracy (Wereley and Meinhart 2001; Wereley et al. 2002).

An essential difference between macro and μ-PIV is the form of illumination used. μ-PIV uses volume illumination and not sheet illumination. In volume illumination, all of the particles in the viewing volume are illuminated. In macroscopic PIV a thin laser sheet usually ensures a very good signal-to-noise ratio (SNR) and that out-of-focus particles do not contribute to velocimetry measurements. For volume illumination in μ-PIV, depth of focus (DOF) is not used to judge an unfocused particle's contribution to velocimetry measurements. Instead, the appropriate metric is the depth of correlation (DOC). DOC is defined as twice the distance that a particle can be positioned from the object plane so that the intensity along the optical axis is an arbitrarily specified fraction of its focused intensity, denoted by ξ (Meinhart et al. 2000). At axial distances from the object plane greater than the DOC the particle becomes sufficiently out of focus, so that it no longer contributes significantly to the signal peak in the correlation function. If we take $\xi = 0.1$ the DOC (δ_{corr}) can be approximated as (Meinhart et al. 2000).

$$\delta_{\text{corr}} = \frac{3n\lambda}{NA^2} + \frac{2.16d_{\text{p}}}{\tan\theta} + d_{\text{p}} \tag{2}$$

where d_{p} is the particle size, n is the refractive index of the fluid between the microfluidic device and the objective lens, NA is the numerical aperture of the objective len and θ is related to NA by $NA = n\sin\theta$ and λ is the wavelength of light.

6 Experimental

6.1 Fabrication of parallel electrode microfluidic chamber

Figure 3 illustrates the design of the parallel electrode microfluidic chamber. The top and bottom surfaces of the chamber are made using ITO coated glass. Thus the channel base and lid serve as electrodes. ITO-coated glass coverslips (~170 μm thick) were used for the bottom electrode while the top electrode was made from ITO-coated glass (~0.7 mm thick). The ITO electrodes were separated by a 50 μm insulating spacer with microfluidic features. The image acquisition area is placed approximately in the middle of the channel. The spacer does not influence the local electric field in the experimental area since the imaging area (150 μm × 112 μm) is small compared to the channel width (w ~ 1.5 mm) and it's centered between the channel side walls.

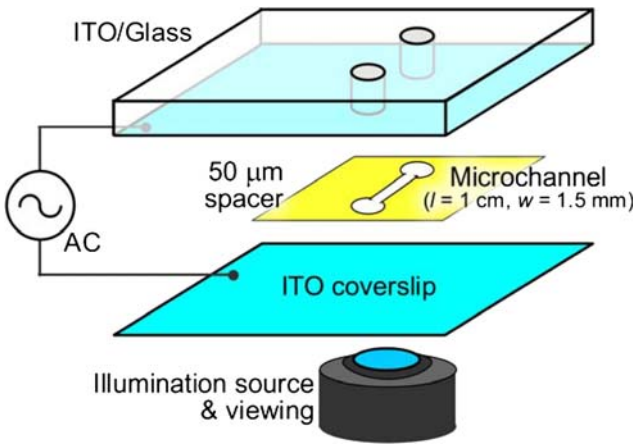

Fig. 3 An illustration of the microchannel used for the microvortex experiments. The bottom electrode is ~170 μm thick to allow access to a high numerical aperture lens. The length of the microchannel is approximately 1 cm and the width is 1.5 mm. The ports on the top electrode allow fluid to enter the microchannel

6.2 Flow visualization and velocimetry

An inverted Nikon TE2000U microscope equipped with a Nikon 60× water-immersion objective lens (1.2 NA and 0.27 mm working distance) is utilized for visualizing fluid flow. Since a high NA objective lens was used for this investigation coverslips were used for the bottom channel-wall. An AC signal was biased across the channel, generating a uniform electric field in the experimental viewing area. A focused laser spot is created by focusing a laser through the viewing objective lens. In the present investigation we used a 1,064 nm Nd:YAG laser. The laser has an inherent 5% variability in power output. All references to laser power here are with respect to the back aperture of the microscope objective lens.

For μ-PIV analysis, 300 nm red fluorescent particles (Duke Scientific, CA, USA) were used as tracers. Samples were prepared by mixing the particles with about 20 μM solution of KCl in DI water. The conductivity of the KCl solution was measured before experiments and ranged from 0.33 to 0.45 mS/m. The images were captured with an interline transfer charge coupled device (CCD) camera (Coolsnap HQ, Photometrics, Roper Scientific Inc.). The camera has a 1,392 × 1,040 element CCD at a 6.45 μm × 6.45 μm pixel pitch. Time interval between successive images was 0.15 s. Enhanced Digital Particle Image Velocimetry (Edpiv), a software package developed by Dr. Lichuan Gui (Gui and Merzkirch 1998), was used for the μ-PIV analysis. For all results shown here the flow characteristics were analyzed in a plane parallel to the bottom electrode and at an approximate distance of 8 μm above the bottom surface as shown in Fig. 4.

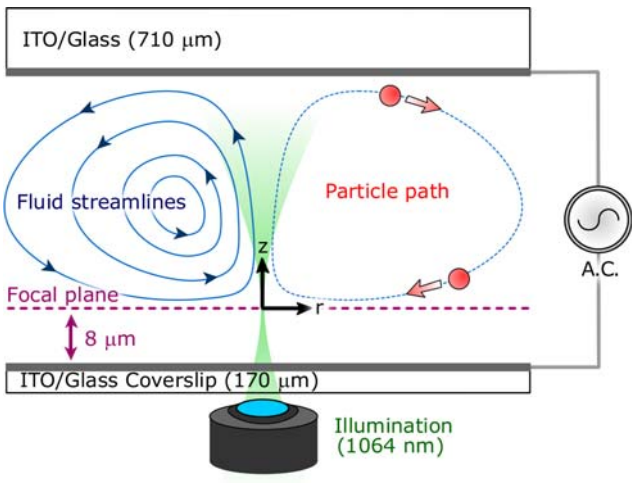

Fig. 4 An illustration showing location of the measurement plane for flow visualization and μPIV experiments. Note that the measurement plane, focal plane and plane of laser focus are synonymous

6.3 Dielectrophoresis experiments

For OEMV analysis within interdigitated electrodes, electrodes were purchased from ABTech Scientific (Richmond, Virginia, USA). The electrodes were fabricated on 0.7 mm borosilicate glass, patterned with ITO, and the electrodes were insulated with 0.5 μm thick layer of silicon nitride. The interdigitated electrodes were 20 μm in digit width and spacing. A 50 μm spacer with was used to separate the electrode substrate with a glass coverslip. The same inverted microscope was fitted with a 40× objective lens (0.8 NA and 2 mm working distance) for visualization. Fluorescent latex particles of 1.0 μm (Molecular probes, MD, USA) were suspended in the same low-conductivity water solution. Simultaneous OEMV and DEP experiments were conducted with an applied high-frequency (≥2 MHz) AC signal. At these conditions the particles will experience negative DEP.

7 Toroidal vortices in the planar electrode system

7.1 Microvortex results

Initial flow visualization experiments were performed with a low concentration of 2 μm beads in the same low-molarity KCl solution. The applied AC signal was 9 V_{pp} and 50 kHz with 20 mW illumination. The exposure time was 100 ms with 200 ms between each acquired image. Figure 5 shows the three-dimensional structure of the micro-vortex. In this sequence of images the particle begins on the focal plane, moving towards the illumination center. This particle experiences out-of-plane (z-direction) motion and translates out-of-focus. The particle moves away and comes back into focus as it approaches the illumination center. Thus, the particle appears to be traveling along a closed streamline. In fact these particles have exceedingly stable orbits and if ideal conditions are maintained (no bulk fluid flow, no vibration) they maintain their periodic orbits indefinitely. The presence of these closed orbits establishes the 3-D behavior of electrothermal flow. Note that the defocused images in Fig. 5 differ slightly from Fig. 2b, which was imaged in air.

Figure 6 illustrates the fluid flow behavior in the focal plane using particle pathlines of 1 μm fluorescent beads (Molecular probes, MD, USA). Figure 6a demonstrates pathlines created by superimposing 50 consecutive images. Similarly Fig. 6b, c were created by superimposing 100 and 200 consecutive images, respectively. In the measurement plane, the laser is focused into a diffraction limited spot of approximately 1 μm diameter. The origin denotes the location of the laser focus. The flow is steady-state and hence particle pathlines and fluid streamlines are

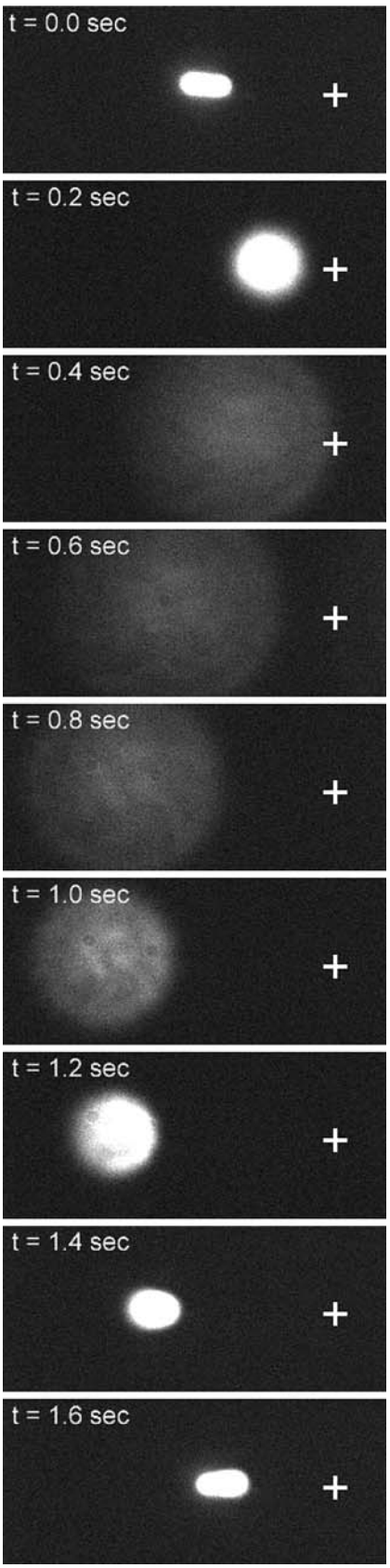

◀ **Fig. 5** A large tracer particle (2 μm) is caught within the vortex and follows the fluid streamlines with periodic motion. The particle initially moves towards the illumination center (denoted by '+'), goes out of focus as it moves away, and moves towards the focused laser spot again as it comes back into focus

identical. A few characteristics of the fluid flow can be immediately concluded from Fig. 6. First is that the flow in the viewing plane resembles a sink, with its center occurring at the laser focal point. Two zones of fluid flow can also be distinguished. The 'sink-type' (roughly external to the dashed circle) zone shows primarily a radial flow with very low angular velocities. Internal to the dashed circle is the zone with high z-direction velocities. Even with the progress of time particle pathlines are nearly absent from the interior of the dashed circle. As the fluid here has high z-direction velocity, particles experience significant out-of-plane motion and thus particle pathlines appear to terminate in this region's periphery. As the particles develop significant z-direction velocities we can expect a distortion of the in-plane, radial velocity μ-PIV measurements.

All of the μ-PIV measurements were carried out in the same measurement plane (Fig. 4) with 300 nm fluorescent particles and a constant illumination intensity of 20 mW. The microvortex was first analyzed by keeping the applied AC frequency constant (100 kHz) and varying its voltage. Figure 7 shows the in-plane radial velocity from the μ-PIV analysis of these experiments, where radial location (r) is with respect to the location of the laser spot center. The radial velocity in the sink-type region increases with decreasing radial position until it reaches a maximum before decreasing again. Closer to the laser focus the radial velocity decreases due to the very high z-direction fluid velocities. Significant z-direction velocities in this region distort the in-plane velocity measurements. The whole velocity profile increases in magnitude with an increase in applied voltage; this value roughly doubles as the square of the voltage (V^2) doubles (Fig. 7). The radial location at which the velocity profile reached a maximum is denoted by R_v and the corresponding velocity by $v(R_v)$. The velocities from Fig. 7 are normalized with respect to $v(R_v)$ and plotted in Fig. 8 (without the $V = 5.65\ V_{pp}$ data). Note that radial velocities are negative in Fig. 7 as particles move inwards, while they become positive in Fig. 8 due to normalization. The velocity maximum is reached approximately at the same radial location (R_v) with the normalized velocity plot maintaining its overall shape. Hence the shape of such a vortex can be characterized by R_v ($\sim$11.5 μm), which is independent of electric field strength. Due to the systematic errors caused by the large out of plane velocities at radial locations less than R_v, trends for $r < R_v$ were not analyzed. The sink-type region demonstrates a radial velocity decay of the type $v_r = a/r + b$, where a and b are constants. The goodness of

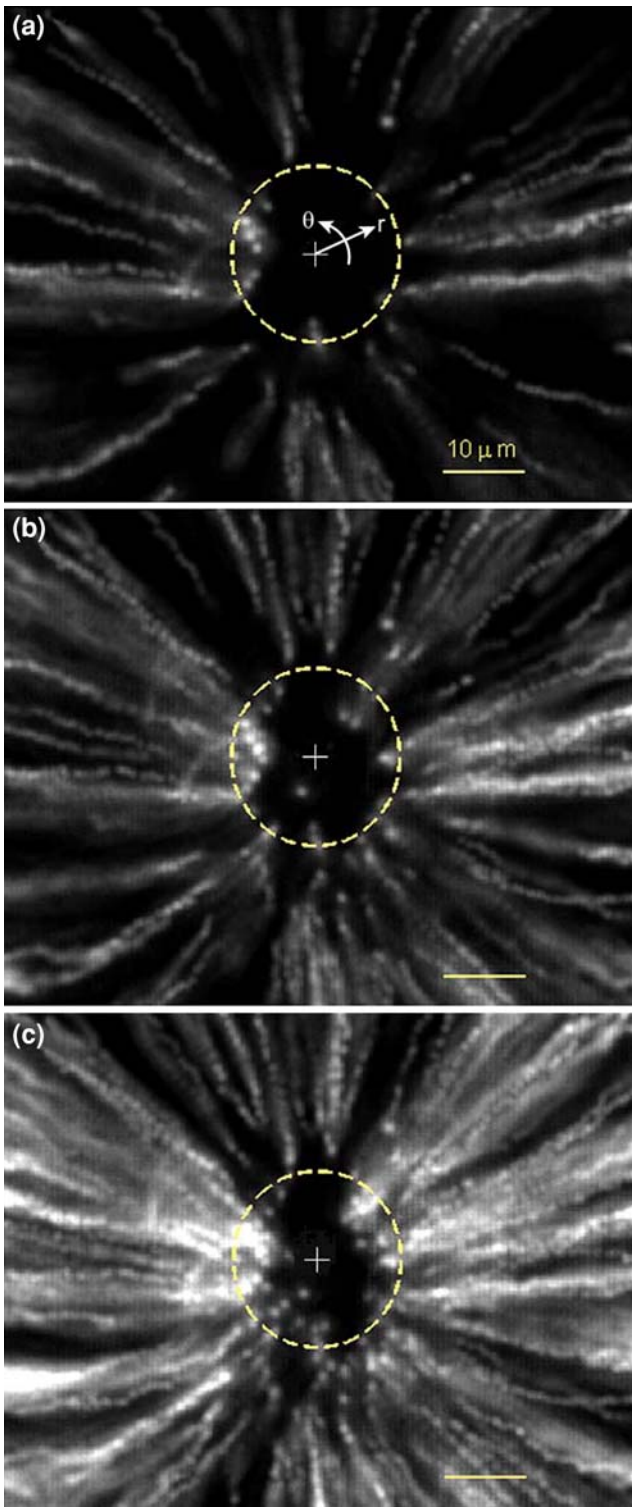

Fig. 6 Time evolution of particle pathlines in the plane of measurement (Fig. 4). **a** 50 overlapped images of tracer particles creating pathlines showing inward fluid motion of the vortex. **b** 100 overlapped images of tracer particles. **c** 200 overlapped images of tracer particles. The central region bound by the *dashed circle* experiences significant out-of-plane effects as particles develop high z-direction velocities. The laser focal point is approximately at the center of the *dashed circle*

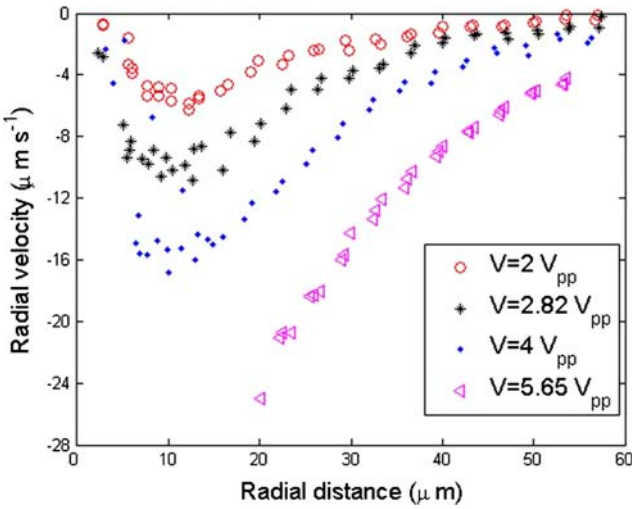

Fig. 7 μ-PIV analysis of the velocity field for vortex flow near the electrode surface. V_{pp} represents the applied peak-to-peak AC bias. All measurements were performed at f = 100 kHz and P = 20 mW

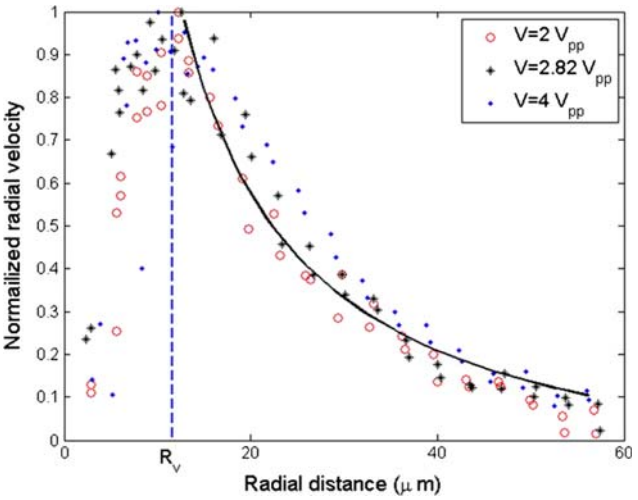

Fig. 8 Normalized plot for radial velocities. The *curve* represents best fit sink type behavior, i.e. $v_r = a/r + b$

fit is characterized by R^2, and its high value of 0.94 suggests the adequacy of the model. In Fig. 8, the values of a and b are 7.32 and −0.16 respectively.

The frequency-dependent behavior of the microfluidic vortex was investigated with a constant voltage of 4 V_{pp}. In the low frequency regime (30–50 kHz) velocity does not change significantly (Fig. 9). However, at very high frequencies (>5 MHz) fluid velocity decreased significantly and was barely noticeable as the movement of the tracer particles was dominated by Brownian motion. This follows expected theory, as the Coulomb term for the fluid body force decreases with increasing frequency. Further, it seems Brownian motion dominates the dielectric fluid body force for our experimental parameters at these high frequencies.

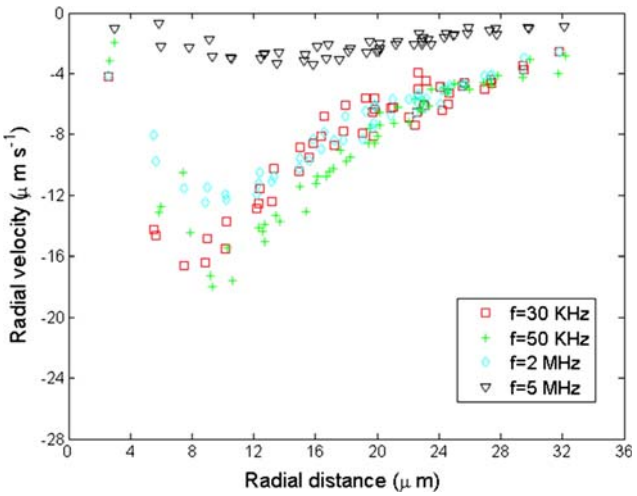

Fig. 9 Velocimetry results as a function of frequency. All measurements were performed at $V = 4\ V_{pp}$ and $P = 20$ mW

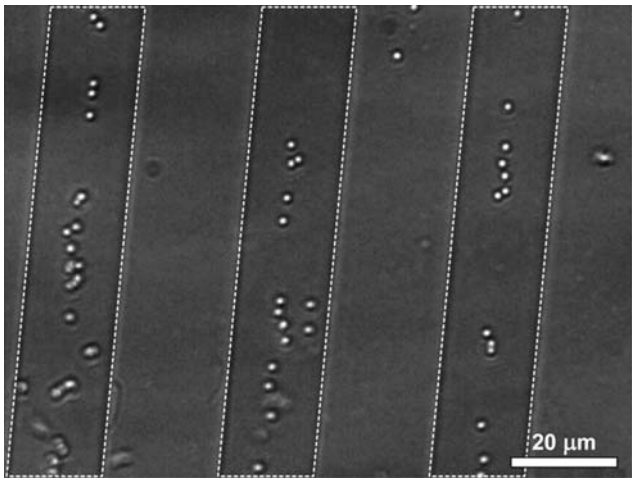

Fig. 10 Latex particles experiencing negative DEP in the absence of laser heating at $f = 3$ MHz and $V = 9\ V_{pp}$. The *dotted rectangles* indicate the location of the interdigitated ITO electrode strips. Notice that the particles are trapped above the electrodes as illustrated in Fig. 1

7.2 μ-PIV parameters

In Eq. (2) we saw that the depth of correlation (δ_{corr}) strongly depends on numerical aperture of the objective lens and particle size (d_p). For a 300 nm particle imaged with a 60× water-immersion lens, the DOC is ~2.3 μm. On average nine particle images were present per 64 × 64 pixel^2 interrogation window. Correlation averaging greatly improves SNR measurements (Wereley et al. 2002) and SNR values greater than 1.4 were achieved through correlation averaging of 200 images.

8 Interdigitated electrodes

Now, we discuss the results obtained from the interdigitated electrode configuration. We immediately observed that the velocity and direction of the induced OEMV varies with the position of the laser spot. Additionally, at low-frequencies (<50 kHz), electrohydrodynamic fluid motion at the electrode edges was readily apparent. Although OEMV did occur with interdigitated electrodes, fluid velocities were difficult to quantify as the strong electric field gradients generate considerable dielectrophoretic forces that compete with electrohydrodynamic fluid drag forces. To qualitatively demonstrate the effect of the OEMV, experiments were repeated with and without laser irradiation. Figure 10 shows the behavior of 1 μm latex particles with the interdigitated electrode configuration without any laser irradiation. With an applied AC signal of 9 V_{pp} and 3 MHz and fluid conductivity of 3.34e-4 S/m the particles experienced negative dielectrophoresis and aggregate above the electrode digits. In the absence of any other external force each electrode strip is equally probable to accumulate particles.

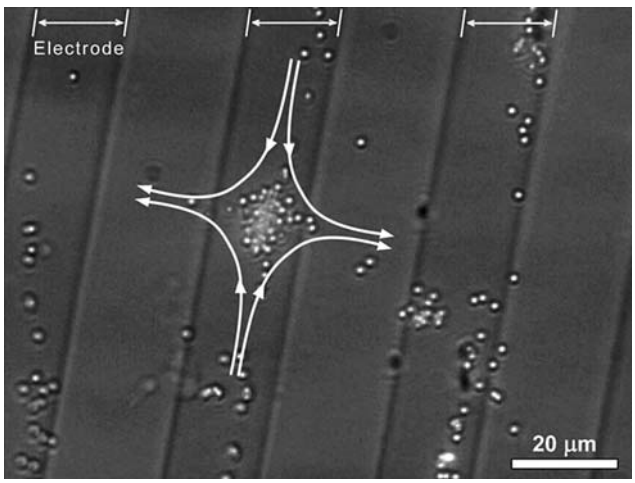

Fig. 11 Illustrated behavior of the OEMV for interdigitated electrodes with the laser focal point located in the middle of an electrode digit. Electrodes are labeled with *arrows* at the top of the figure. The direction of the fluid flow is depicted with *curved arrows* with the laser focus occurring in the middle of the vortex. Particles are pushed with the fluid towards the illumination spot and a few are ejected perpendicular to the edge of the electrode

Figure 11 illustrates the behavior of the OEMV and particles once laser irradiation is applied to the interdigitated electrodes with the laser focus located in the middle of an electrode strip (approximately in the middle of the dashed circle). Here, the fluid flow of the OEMV is illustrated with curved arrows. The structure of the vortex

differs in orientation compared to the parallel electrode setup in Fig. 4. While the vortex draws in fluid along the length of the electrodes, fluid is discharged perpendicular to the electrode edges. Particles tend to drag with the fluid, along the middle of the electrode strip, to form a clump at the location of the laser spot (Fig. 12(a–c)). Occasionally particles will be ejected from the clump in the outward direction of the OEMV due to fluid drag. However, due to DEP forces the majority of the particles remain clustered at the center of the vortex. Further, the particles experiencing negative DEP on the neighboring electrodes were not completely centered on their respective electrode digit and were pushed away by fluid drag originating from the vortex. The conditions for these experiments were a laser illumination of 40 mW and an AC signal of 8 V_{pp} and 2 MHz.

A highly focused laser beam can also lead to optical tweezing. However, the presence of an agglomeration of particles should not be confused with optical trapping of beads. Optical tweezers typically employ a laser beam focused to a diffraction limited spot (Ashkin 1997; Kumar et al. 2008) and this spot acts as the trapping zone. For 1,064 nm, this spot size is approximately 1 μm in diameter. Typically, while trapping beads of the same size (∼1 μm), the trapping region can accommodate only one bead.

9 Electrohydrodynamic analysis

The effect of thermal convection was studied by observing fluid flow without applying a potential difference. Convection currents were extremely weak at P = 20 mW and could be seen only in the close proximity of the laser focus. Thus the presence of an electric field is essential to create such a vortex-like structure. Electric fields typically induce a body force on a fluid through electro-osmotic effects (Ramos et al. 1998; Ajdari 2000) or electrothermal (Green et al. 2000) mechanisms. The parallel electrode configuration does not naturally possess the tangential electric fields required to produce electro-osmotic effects. Microfluidic vortices were present at a frequency of 2 MHz (Fig. 10); AC electro-osmosis does not influence fluid motion at 2 MHz as it can be neglected at frequencies >100 kHz for low-conductivity mediums (Morgan and Green 2003). In addition, the general profile of the microfluidic vortex does not significantly change with voltages or frequencies in this investigation. Therefore, electrothermal effects dominate and other electrokinetic effects do not interfere.

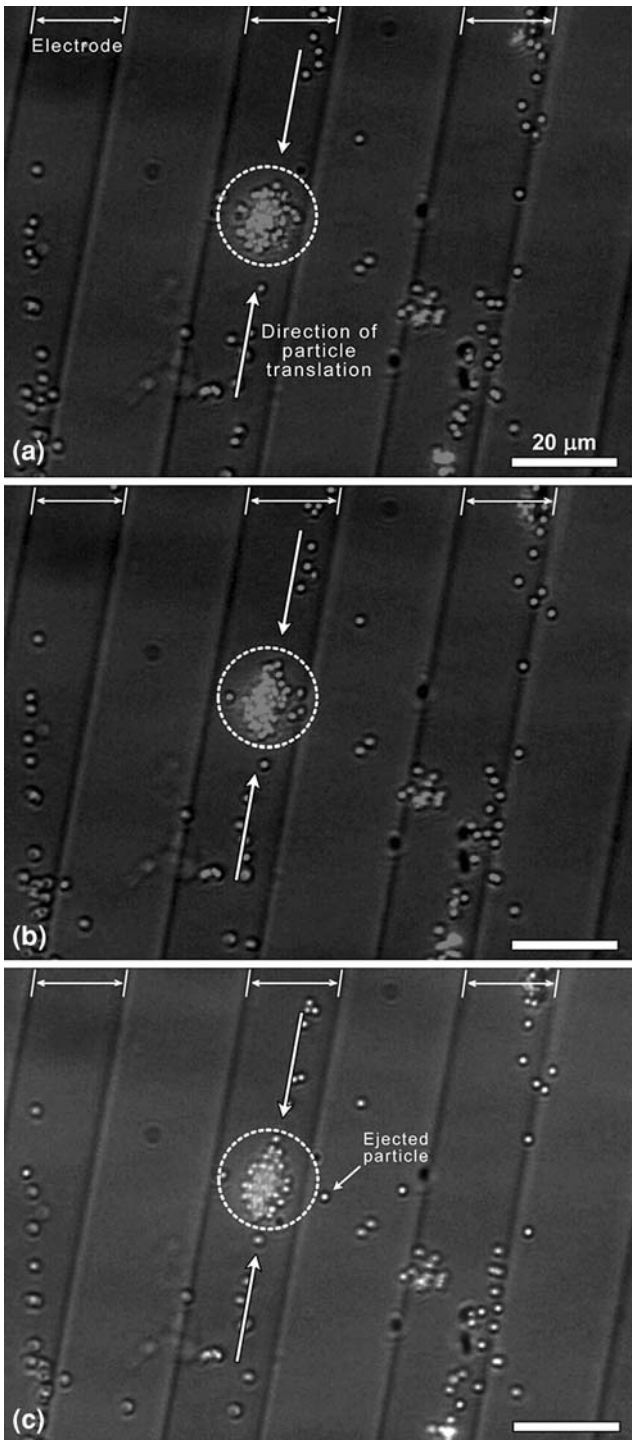

Fig. 12 Effect of the OEMV laser spot on latex particles (1.0 μm) for interdigitated electrodes at V = 8 V_{pp}, f = 2 MHz and P = 40 mW. Electrodes are labeled with arrows at the top of the figure. These frames are taken at (**a**) t = 0 s (b) t = 1.26 s and (c) t = 2.8 s. Particle groups are brought in due to fluid drag (*larger arrows*) by the OEMV and remain clustered due to negative DEP forces (*dashed circle*). Note the ejected particle in (**c**)

10 Conclusions

Intense laser irradiation in the presence of uniform or non-uniform electric fields can generate strong fluid vortices. Even in the simple case of a uniform electric field, strong microfluidic vortices with a three-dimensional structure can be generated. These three-dimensional vortices can perhaps be utilized for microfluidic mixing. Compared to active-mixers these vortices can be employed without the need of any invasive, agitating mechanical components. In case of an interdigitated electrode configuration, these vortices can complicate dielectrophoretic particle capture. Thus any effort to combine OTs and DEP for simultaneous operation needs to take into account these induced vortices.

Acknowledgments We would like to acknowledge support from NSF Grant CMMI-0654031. Aloke Kumar acknowledges partial support from the Adelberg Fellowship, Purdue University. S.J.W. acknowledges support under a National Science Foundation Graduate Research Fellowship.

References

Ajdari A (2000) Pumping liquids using asymmetric electrode arrays. Phys Rev E 61:R45–R48

Ashkin A (1997) Optical trapping and manipulation of neutral particles using lasers. Proc Natl Acad Sci USA 94:4853–4860

Ashkin A, Dziedzic JM, Yamane T (1987) Optical trapping and manipulation of single cells using infrared-laser beams. Nature 330:769–771

Chakraborty S (2008) Electrothermal effects. Encyclopedia of Microfluidics and Nanofluidics. L. Dongqing, Springer, Berlin

Chiou PY, Ohta AT, Wu MC (2005) Massively parallel manipulation of single cells and microparticles using optical images. Nature 436:370–372

Curtin DM, Newport DT, Davies MR (2006) Utilising μ-PIV and pressure measurements to determine the viscosity of a DNA solution in a microchannel. Exp Thermal Fluid Sci 30:843–852

Figeys D, Pinto D (2000) Lab-on-a-chip: a revolution in biological and medical sciences. Anal Chem 72:330A–335A

Fuhr G, Schnelle T, Müller T, Hitzler H, Monajembashi S, Greulich KO (1998) Force measurements of optical tweezers in electro-optical cages. Appl Phys a-Mat Sci Process 67:385–390

Green NG, Ramos A, Gonzalez A, Castellanos A, Morgan H (2000) Electric field induced fluid flow on microelectrodes: the effect of illumination. J Phys D Appl Phys 33:L13–L17

Green NG, Ramos A, Gonzalez A, Castellanos A, Morgan H (2001) Electrothermally induced fluid flow on microelectrodes. J Electrostat 53:71–87

Gui L, Merzkirch W (1998) Generating arbitrarily sized interrogation windows for correlation-based analysis of particle image velocimetry recordings. Exp Fluids 24:66–69

Hwang H, Oh Y, Kim JJ, Choi W, Park JK, Kim SH, Jang J (2008) Reduction of nonspecific surface-particle interactions in opto-electronic tweezers. Appl Phys Lett 92:024108–024110

Inouâe S, Spring KR (1997) Video microscopy: the fundamentals. Plenum Press, New York

Jones TB (1995) Electromechanics of particles. Cambridge University Press, Cambridge

Koch M, Evans A, Brunnschweiler A (2000) Microfluidic technology and applications. Research Studies Press, Baldock

Kumar A, Ewing AH, Wereley ST (2008) Optical tweezers for manipulating cells and particles. Encyclopedia of Microfluidics and Nanofluidics. L. Dongqing, Springer, Berlin

Luo R, Sun YF, Peng XF, Yang XY (2006a) Tracking sub-micron fluorescent particles in three dimensions with a microscope objective under non-design optical conditions. Meas Sci Technol 17(6):1358–1366

Luo R,Yang XY, Peng XF, Sun YF (2006b) Three-dimensional tracking of fluorescent particles applied to micro-fluidic measurements. J Micromech Microeng (16)8:1689–1699

Meinhart CD, Wereley ST, Gray MHB (2000) Volume illumination for two-dimensional particle image velocimetry. Meas Sci Technol 11:809–814

Mizuno A, Nishioka M, Ohno Y, Dascalescu LD (1995) Liquid microvortex generated around a laser focal point in an intense high-frequency electric-field. IEEE Trans Ind Appl 31:464–468

Morgan H, Green NG (2003) AC electrokinetics: colloids and nanoparticles. Research Studies Press, Philadelphia

Müller T, Gerardino A, Schnelle T, Shirley SG, Bordoni F, DeGasperis G, Leoni R, Fuhr G (1996) Trapping of micrometre and sub-micrometre particles by high-frequency electric fields and hydrodynamic forces. J Phys D Appl Phys 29:340–349

Nakano M, Katsura S, Touchard GG, Takashima K, Mizuno A (2007) Development of an optoelectrostatic micropump using a focused laser beam in a high-frequency electric field. IEEE Trans Ind Appl 43:232–237

Papagiakoumou E, Pietreanu D, Makropoulou MI, Kovacs E, Serafetinides AA (2006) Evaluation of trapping efficiency of optical tweezers by dielectrophoresis. J Biomed Opt 11:014035-014031–014035-014037.

Pickard JE, Pries AR, Ley K (2006) Micro-PIV measurement of flow fields around adherent leukocytes. FASEB J 20:A1322–A1322

Pohl HA (1978) Dielectrophoresis: the behavior of neutral matter in nonuniform electric fields. Cambridge University Press, Cambridge

Ramos A, Morgan H, Green NG, Castellanos A (1998) Ac electrokinetics: a review of forces in microelectrode structures. J Phys D Appl Phys 31:2338–2353

Reichle C, Schnelle T, Müller T, Leya T, Fuhr G (2000) A new microsystem for automated electrorotation measurements using laser tweezers. Biochim Biophys Acta Bioenerg 1459:218–229

Reichle C, Sparbier K, Müller T, Schnelle T, Walden P, Fuhr G (2001) Combined laser tweezers and dielectric field cage for the analysis of receptor-ligand interactions on single cells. Electrophoresis 22:272–282

Rowe AD, Leake MC, Morgan H, Berry RM (2003) Rapid rotation of micron and submicron dielectric particles measured using optical tweezers. J Modern Optics 50:1539–1554

Santiago JG, Wereley ST, Meinhart CD, Beebe DJ, Adrian RJ (1998) A particle image velocimetry system for microfluidics. Exp Fluids 25:316–319

Schnelle T, Müller T, Reichle C, Fuhr G (2000) Combined dielectrophoretic field cages and laser tweezers for electrorotation. Appl Phys B 70:267–274

Simpson GJ, Wilson CF, Gericke KH, Zare RN (2002) Coupled electrorotation: two proximate microspheres spin in registry with an AC electric field. Chemphyschem 3:416–423

Trau M, Saville DA, Aksay IA (1997) Assembly of colloidal crystals at electrode interfaces. Langmuir 13:6375–6381

Wereley ST, Gui L, Meinhart CD (2002) Advanced algorithms for microscale particle image velocimetry. AIAA J 40:1047–1055

Wereley ST, Meinhart CD (2001) Second-order accurate particle image velocimetry. Exp Fluids 31:258–268

Wu M, Roberts JW, Buckley M (2005) Three-dimensional fluorescent particle tracking at micron-scale using a single camera. Exp Fluids 38(4):461–465